Sensitivity analysis of a Ground-Gen Airborne Wind Energy System design

Sensitivity analysis of a Ground-Gen Airborne Wind Energy System design

Filippo Trevisi, Carlo E.D. Riboldi and Alessandro Croce

Politecnico di Milano, Department of Aerospace Science and Technology, Via La Masa 34, Milano (20156), Italy

E-mail: filippo.trevisi@polimi.it

Abstract. The architecture of a new multidisciplinary design and optimization framework for rigid wing Airborne Wind Energy Systems, named *T-GliDe*, is introduced and a Ground-Gen AWES is analyzed to illustrate the features of the design approach. *T-GliDe* features an optimization module and an uncertainty quantification module, allowing for a number of algorithm-based design techniques. *T-GliDe* performs an AWES design optimizing market-based objective functions, while satisfying constraints related to flight stability. The flight dynamics is modelled with analytical aerodynamic theories, allowing for fast and consistent design evaluations, without the use of time simulation codes and thus of active control. In this work, a reduced optimization problem is run to find optimal working-set points of a Ground-Gen AWES with respect to power production. The reel-out factor and the pitch angle as function of wind speed are considered as design variables and output trends are shown. A variance based sensitivity analysis is then run to investigate how the rigid body eigenvalues are influenced by a set of independent variables. Among the chosen independent variables, a sub-set of variables which bear an impact on the dynamics is identified and they will be considered in future design and optimization activities as design variables.

1. Introduction

Airborne Wind Energy (AWE) is the field of wind energy which aims at harvesting wind power throughout the use of airborne systems. Airborne Wind Energy Systems (AWESs) are classified based on how electricity is generated and on the their flight operations. Power can be generated with a fixed or a moving ground station or on the flying device. The flight operations can be additionally divided into crosswind, tether-aligned and rotational [1]. This paper focuses on the AWESs generating power by flying crosswind with fixed ground-station, called here Ground-Gen AWESs. Moreover, Ground-Gen AWESs can be classified based on the wing type: fixed wings, treated in this work, or soft wings can be used.

To enter the market successfully, AWESs need to prove reliability and robust operations over long time frames, on top of being competitive in the energy market. These requirements shall be considered from the very first stages of an AWE project, when the system design is not fixed and modifications can impact system performances. Bearing this in mind, the present work introduces a new design approach where the AWES is designed based on market metrics, while ensuring good dynamic characteristics, which may enhance controllability and reliability. Based on the theory developed in [2], a multidisciplinary design and optimization framework (*T-GliDe: Tethered Gliding system Design*) has been built with the aim of designing an AWES

maximizing power production or minimizing cost-related objective functions, while satisfying constraints related to flight stability on top of conventional constraints. This approach differs from optimization approaches based on low-fidelity models [3, 4] or on approaches which focus on the aero-structural design for specific design load cases [5, 6], which typically do not include flight dynamics, and from approaches which find power output and loads by running time simulations, which include control [7].

In this work, the architecture of *T-GliDe* is introduced and a sensitivity analysis on an example is presented to explore the design space. The aim of the sensitivity analysis is to give an understanding of the design space, considering stability features, and show how independent variables influence relevant outputs. Independent variables which have an impact on the design will be considered as design variables in future design and optimization activities.

This paper is organized as follows: In Section 2, the architecture of *T-GliDe* is introduced. In Section 3, the optimal working set-points of an AWES are found and trends are studied as function of wind speed. In Section 4, a variance based sensitivity analysis on a set of independent variables is carried out and the design space explored. Finally, in Section 5 the main conclusions of this work are summarized and future works introduced.

2. T-GliDe architecture

T-GliDe is being developed to feature many levels of fidelity inside the same framework. At this stage of development, low fidelity models are included allowing for a conceptual design of the system. Low-fidelity models are useful to quickly evaluate designs and explore the design space. Higher fidelity models are intended to be included later, when dealing with a detailed design of the AWES.

In Figure 1, the general architecture is displayed. The framework features an optimization module and an uncertainty quantification module. When used separately, optimization problems can be solved to obtain a design maximising a marked based objective function for given values of model parameters. An example of a reduced optimization problem is given in Section 3. Sensitivity analyses on specific designs can be performed without solving the optimization problem. This informs on the sensitivity of the design on a set of independent variables. An example of sensitivity analysis on a given design is given in Section 4. When the two modules are used together, sensitivity analyses on the optimization problem itself are performed. This give an understanding on how optimal designs vary, as shown in [4]. Therefore, the current framework allows for a number of combinations of different algorithm-based design techniques which might be used at different design stages and for different purposes.

2.1. Optimization problem

An optimization problem can be written in generic form as

$$\begin{aligned} \underset{\boldsymbol{x}}{\text{minimize}} \quad & f(\boldsymbol{x}) \\ \text{subject to} \quad & \boldsymbol{l} \leq \boldsymbol{x} \leq \boldsymbol{u} \\ & \boldsymbol{g}(\boldsymbol{x}) \leq 0 \\ & \boldsymbol{h}(\boldsymbol{x}) = 0 \end{aligned} \tag{1}$$

Where $\boldsymbol{x}$ are the design variables, f the objective function, $\boldsymbol{l}$ and $\boldsymbol{u}$ the lower and upper bounds of $\boldsymbol{x}$, $\boldsymbol{g}$ the inequality and $\boldsymbol{h}$ the equality constraints. In this work, the gradient-based algorithm Sequential Quadratic Programming (SQP), implemented in the function *fmincon* [8] in MATLAB®, is used. The framework is however not restricted to any specific optimization algorithm and, according to the problem, different algorithms might be used.

Considering the present problem, design variables can be divided into geometrical, i.e. those defining the geometrical characteristics of the system, and operational, defining the working

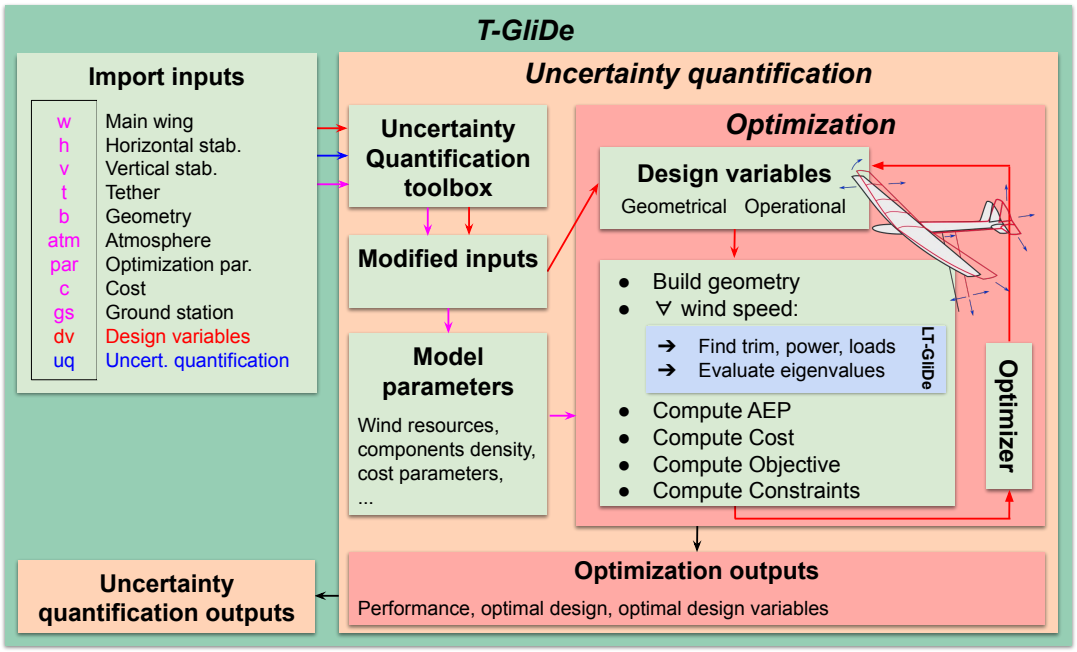

Figure 1. *T-GliDe* (Tethered Gliding system Design) architecture.

set-point as function of wind speed. Part of this work concerns the identification of a pertinent set of design variables for the optimization.

2.1.1. Model The physical model in *T-GliDe* is based on *LT-GliDe* (Linearized Tethered Gliding system Dynamics) [2]. *T-GliDe* is not restricted to a generation type (i.e. Fly-Gen or Ground-Gen) and will be used to analyse and design both systems. *LT-GliDe* is initialized with geometrical and inertial characteristics of the AWES and with operational parameters describing the working set-point (i.e. reel-out wind speed and pitch angle in this work) as function of wind speed. At this stage of development, inertial characteristics of the aircraft are estimated with a historical regression approach, following the formulation proposed in [9] or kept constant. Holding inertial characteristics constant tells the designer on how aerodynamic features alone influence the design.

LT-GliDe assumes the dynamic problem to be axial-symmetric by considering the fluctuating terms over the loop as disturbances. Figure 2 shows the trajectory, where the component of the gravitational force on the rotor plane ($\mathbf{g}\cos\beta$) and the component of the wind velocity on the rotor plane ($V_w \sin\beta$) are the fluctuating terms. In this way, the AWES states over the circular trajectory can be described with a unique steady state. This steady state is considered as representative of the dynamics over the loop and it is used to evaluate trim, loads and power. The dynamics of the system in the circular trajectory is then linearized about the steady state. The aerodynamic derivatives are computed using analytical aerodynamics theories and the stability of the system is then studied by evaluating the eigenvalues of the linearized problem. *LT-GliDe* has been developed and implemented to be coupled with design tools: the analytical formulation allows for extremely fast and consistent design evaluations.

At each wind speed, *LT-GliDe* finds the trim conditions, the loads and the power output. As this work involves Ground-Gen AWESs, the reel-out velocity V_{ro} is included in the velocity triangle and the power is estimated by the product of tether force and reel-out velocity. Once the power and the loads are evaluated, the annual energy production (AEP) and the costs related

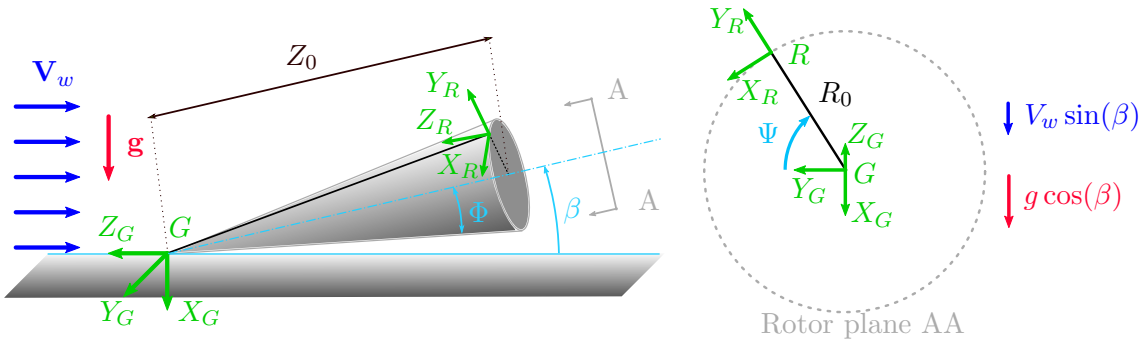

Figure 2. Ground coordinate system $\mathcal{F}_G$ and rotating coordinate system $\mathcal{F}_R$ in *LT-GliDe* [2].

to the design are computed accordingly. The cost model available at this stage of development was previously introduced in [10], while a new updated cost model is being developed and will be presented in future works. Finally, the reel-in phase is modelled with a simplified method [11] assuming a straight trajectory with a constant reel-in speed.

2.1.2. Objective functions A number of objective functions can be used in the optimization. Table 1 summarizes the objective functions available at the current stage. UF is an objective function which might be used for systems without power generation. As different objective functions might lead to different optimal designs, in future works different metrics will be compared and other additional objectives beyond LCoE included [12].

Table 1. Objective functions currently available in T-GliDe.

Objective	Description
CF	Capacity Factor
LCoE	Levelized Cost of Energy
II	Economic Profit
UF	Velocity Factor: Integral of the longitudinal velocity times the wind distribution

2.1.3. Constraints Relevant constraints should be included in the optimization problem. The lift coefficient of the main wing, the longitudinal velocity u_0, the stress acting on the tether σ and the power generation during reel-out phase P_{out} are bounded to an upper level.

On top of these conventional constraints for wind energy, constraints related to the rigid body dynamics at each wind speed are included. In particular, the damping ratio of each eigenmode shall be higher than a given value ζ_{min}. The damping ratio ζ is defined as

$$\zeta^2 = \frac{1}{1 + \left(\frac{\mathrm{Im}(\lambda)}{\mathrm{Re}(\lambda)}\right)^2}. \tag{2}$$

The slope m in the real-imaginary plane of the line given by the minimum damping ratio ζ_{min} is

$$m = \frac{\mathrm{Im}(\lambda)}{\mathrm{Re}(\lambda)} = -\sqrt{\frac{1}{\zeta_{min}^2} - 1}. \tag{3}$$

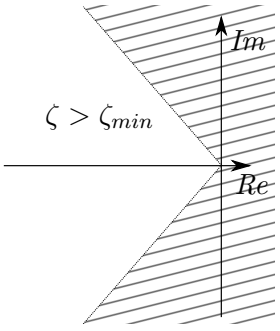

Figure 3. Graphical representation of the stability constraint.

Therefore, the stability constraints impose that the eigenvalues shall be located on the left of the limit line, as shown in Figure 3

$$\boldsymbol{g}_\zeta(\boldsymbol{x}) = |Im(\boldsymbol{\lambda})| - m \cdot Re(\boldsymbol{\lambda}) \leq 0. \tag{4}$$

2.2. Uncertainty quantification

At this stage of development, the uncertainty quantification toolbox *UQLab*[13] is included and can be used to perform local and global sensitivity analyses. Sensitivity analyses can be performed on the optimization problem or on a given design. In this work, a sensitivity analysis is carried out to identify how independent variables influence the design.

3. T-GliDe results: finding optimal working set-points

In this work, an ultra-light aircraft, *Zefiro* [2], is used as a baseline to introduce trends and perform a sensitivity analysis on some independent variables.

In this section, a reduced optimization, where only operational design variables are considered, is run to find the optimal working set-points as function of wind speed. The pitch angle θ (Angle which brings from the body coordinate system $\mathcal{F}_B$ to the stability coo. system $\mathcal{F}_S$ [2]) and the reel-out factor $\gamma_{ro} = \frac{V_{ro}}{V_w}$ as function of wind speed are considered as design variables. The optimizer, in this case, looks for the working set-points in order to maximize power production while satisfying constraints. To introduce results with an increasing level of complexity and since they do not primarily impact the results of this work, the elevation angle β and wind shear are not considered here.

In Figure 4, the power output during the reel-out phase P_{out} and the cycle power P are displayed. The power produced during the reel-out phase is constrained and rated power is reached at 10 m/s. At $V_w = 8$ m/s, the reel-out power is $P_{out} = 139$ kW. The analytic expression for the optimal power production is [10]

$$P_{out} = \frac{1}{2}\rho(C_{L,w}A_w + C_{L,h}A_h)G^2V_w^3\gamma_{ro}(1-\gamma_{ro})^2 = 139 \text{ kW}. \tag{5}$$

Where ρ is the air density, $C_{L,w}$ and $C_{L,h}$ the lift coefficient of main wing and horizontal stabilizer, A_w and A_h the wing area of of main wing and horizontal stabilizer and G the system glide ratio, which is assumed to be high.

In Figure 5, the tether stress is shown as function of wind speed. The tether stress reaches the upper bound at 9.5 m/s and it is capped until 12 m/s. At $V_w = 8$ m/s, the reel-out tether force is $T_{out} = 61$ kN; the component of the reel-out force along the Z_R axis (see Figure 2) is $T_{out}\cos\Phi = 58$ kN. This latter value should be compared with the analytic expression [10]

$$T_{out} = \frac{1}{2}\rho(C_{L,w}A_w + C_{L,h}A_h)G^2V_w^2(1-\gamma_{ro})^2 = 58 \text{ kN}, \tag{6}$$

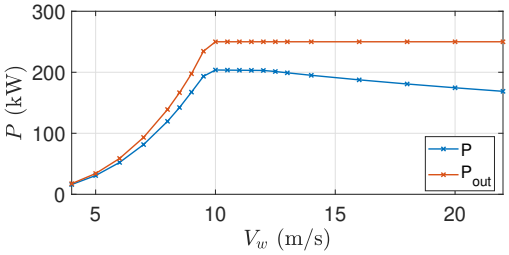

Figure 4. Power output during the reel-out phase P_{out} and cycle power P.

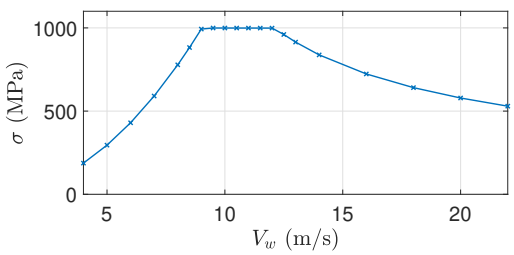

Figure 5. Tether stress as function of wind speed.

which assumes a linear crosswind motion.

In Figure 6 the reel-out factor γ_{ro} and the reel-out velocity V_{ro} as function of wind speed are shown. Until 9 m/s, γ_{ro} has a linear trend. When the maximum tether stress is reached, the optimizer looks for higher γ_{ro}, which result in a constant reel-out velocity until the tether stress is not constrained any more ($V_w = 12$ m/s). Indeed, the reel-out power, which is constrained to a constant, is the multiplication of tether force, which is constrained to a constant, and reel-out velocity, which can vary unconstrained and it is set to a constant by the optimizer. In Figure 7, the pitch angle as function of wind speed is shown. After rated power is reached, the aircraft pitches into the wind to reduced the angle of attack and consequently the lift coefficient, as shown in Figure 8. The lift coefficient of the horizontal and vertical tail are found by trimming the kite and they have similar trends to the main wing lift coefficient.

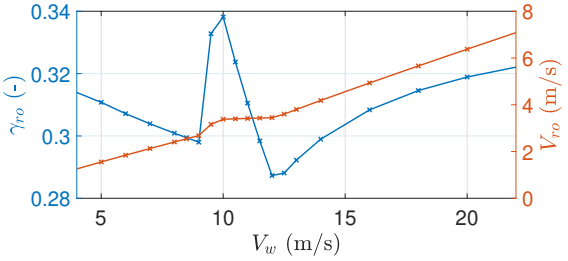

Figure 6. Reel-out factor and velocity as function of wind speed.

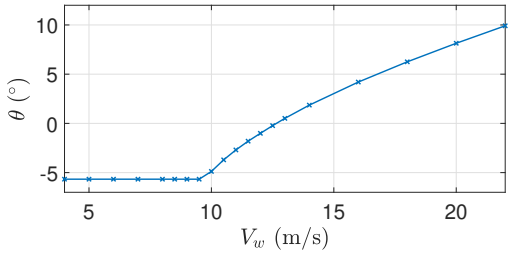

Figure 7. Pitch angle as function of wind speed.

Finally, Figure 9 shows the longitudinal velocity of the aircraft in the circular trajectory. The slope of the velocity as function of wind speed changes when the tether stress becomes constrained and from $V_w = 12.5$ m/s the longitudinal velocity is constrained to a maximum value of 90 m/s.

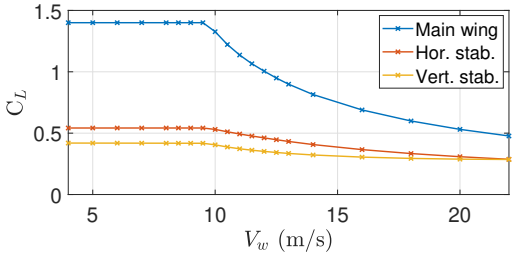

Figure 8. Trimmed lift coefficients of the main wing and vertical and horizontal tail.

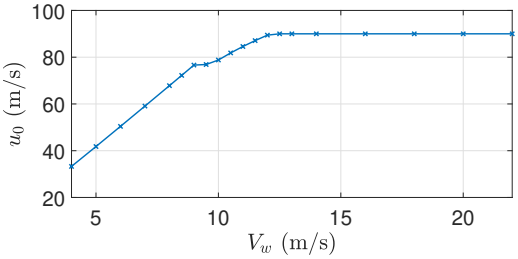

Figure 9. Longitudinal velocity of the aircraft in the circular trajectory.

As introduced in Section 2.1.3, the rigid body eigenvalues of the AWESs are found by *LTGliDe* and in a complete optimization problem their damping ratio will be constrained. As this reduced optimization does not modify the geometry, the eigenvalues are just constrained to have a negative real part. However, these constraints are not active. In Figure 10 and 11 they are shown as function of wind speed. The roll subsidence is left out from the plots because it is real and negative. The eigenvalues have different trend before and after certain constraints become active. The short period has a linear trend before rated power and after the eigenvalues collapse to a location. Dutch roll has a linear trend before maximum tether stress is found, then the imaginary part is almost constant. Phugoid has a linear trend before maximum tether

stress is reached. When tether force is maximum, its eigenvalues are concentrated close to the same location and later the imaginary part is almost constant. Positional eigenmode initially decreases its real part and, after rated power, it increases again. Finally, the imaginary part of the pendulum eigenmode, which for a straight crosswind motion can be approximated with [2]

$$\mathrm{Im}(\lambda_{pend}) \approx \omega_{pend} \approx \sqrt{\frac{T}{mL_t^0}}, \tag{7}$$

follows the trend of the tether force.

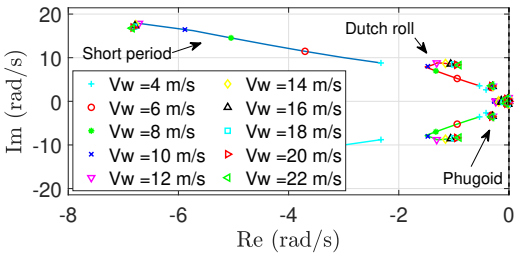

Figure 10. Eigenvalues as function of wind speed.

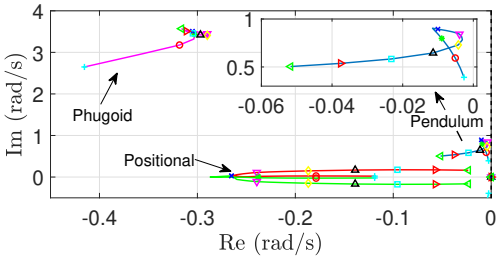

Figure 11. Eigenvalues closer to the positive real axis as function of wind speed.

4. T-Glide results: sensitivity analysis

Before formulating the optimization problem by declaring the design variables, a sensitivity analysis is here performed to study how a set of independent variables influence relevant outputs. Particular emphasis is given on studying how independent variables influence rigid body eigenvalues because this is the novelty introduced within the present approach.

In the previous section, the optimal working set-points of *Zefiro* operated as Ground-Gen AWES are found as function of wind speed. In this section, the AWES operating at $V_w = 8$ m/s is analysed further. A sensitivity analysis is performed to evaluate how the rigid body eigenvalues are influenced by a set of independent variables. The aim of this study is to identify the sub-set of independent variables which bear an impact on the dynamics. These independent variables will be considered in future design and optimization activities as design variables, together with independent variables which impact conventional outputs [4]. It is important to stress here that conventional outputs, such as power and tether force, are left out of this analysis because their analytical expression coincide with *LT-GliDe* outputs (see Eq. (5) and (6)). Therefore studying their dependence on the independent variables could be more intuitively performed by analyzing their analytical expression.

A global sensitivity analysis, and in particular a variance-based decomposition analysis, is carried out to investigate how independent variables variances influence the real and imaginary part of the eigenvalues variances. The total Sobol indices [14] are used to show this dependence. The total Sobol indices represent a measure of how much one output variance is due to one input variance, considering the interaction with other inputs. A high total Sobol index points out that a given input bears a large influence of the relative output globally. To evaluate the Sobol indices, the input space, or the independent variables space in this work, is sampled according to the uncertainties assigned to them and metamodels are built from these evaluations. In this work, *polynomial chaos expansions* are used as metamodels. Sobol indices are finally evaluated using the metamodels. More details of this technique is given in [4].

As this work aims at exploring the design space, a uniform distribution varying form 90 % to 110 % of the nominal value is assigned to the set of independent variables listed in Table 2. The nominal values are given in [2]. As OW_z and OS_z nominal values are null, they are varied from -0.1 m to 0.1 m.

Table 2. Independent variables description.

Var	Description	Var	Description
L_t^0	Average tether length at rest	d_t	Tether diameter
OT_x	Tether attach. position along X_B		
OW_x	Wing root position along X_B	OW_z	Wing root position along Z_B
OS_x	Tail position along X_B	OS_z	Tail position along Z_B
A_w	Main wing area	AR_w	Main wing aspect ratio
Λ	Main wing sweep	Γ	Main wing dihedral
A_h	Horizontal tail area	AR_w	Horizontal tail aspect ratio
A_v	Vertical tail area	AR_w	Vertical tail aspect ratio
m	Total mass	I_x,I_y,I_z	Moments of inertia

In Figure 12, the Sobol indices of the real and the imaginary part of the eigenvalues with respect to the independent variables and for the given uncertainties are shown. A dark color highlights a strong dependence between the input and the output variances.

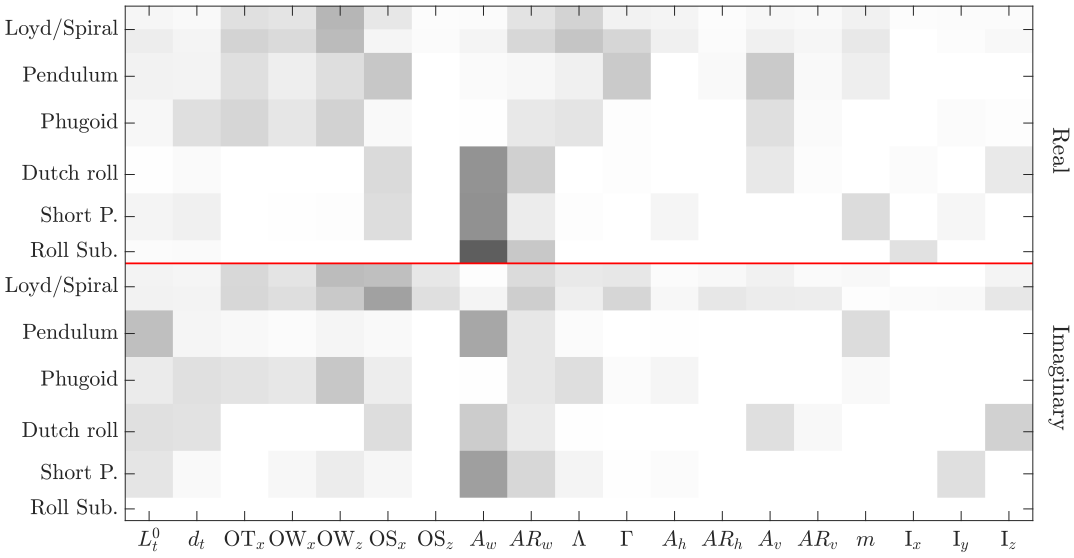

Figure 12. Sobol indices of the real and the imaginary part of the rigid body eigenvalues with respect to the candidate design variables given in Table 2.

To have an example on how to interpret Sobol indices, one can look at the imaginary part of the pendulum eigenvalue $\mathrm{Im}(\lambda_{pend})$. Its variance is strongly influenced by the tether length L_t^0, the main wing area A_w and aspect ratio AR_w and the total mass m variances. Considering Eq. (7), L_t^0 and m are entering in a direct way the approximate estimation of $\mathrm{Im}(\lambda_{pend})$. A_w and AR_w are instead influencing the tether force, which is influencing $\mathrm{Im}(\lambda_{pend})$.

Loyd and spiral mode are gathered together because for some combinations of inputs parameters they merge into positional mode. All complex conjugate eigenvalues have the same Sobol indices. The roll subsidence has no imaginary part, as it is a real eigenvalue.

As the pendulum eigenmode and the phugoid are typically closer to the real positive axis, the stability constraint of these eigenvalues will be likely active when carrying out an optimization. Therefore, focus is given to these modes. The variance of the real part of the pendulum is mainly influenced by the vertical tail area A_v, the main wind dihedral angle Γ, the longitudinal position of the tail OS_x and of the tether attachment OT_x. In Figure 13, the dependent of $\mathrm{Re}(\lambda_{pend})$ on A_v and Γ is shown. This plot is obtained by setting all the other inputs to nominal values. It is found that it is generally beneficial to increase A_v, while the dihedral angle has an optimum value for the pendulum eigenmode. The variance of the real part of the phugoid is influenced by the vertical tail area A_v, the position of the main wing OW, of the tether attachment OT_x and the sweep angle of the main wing Λ. In Figure 14, the damping ratio of the phugoid is shown as function of A_v and the position of the tether attachment along X_B. For the phugoid, it is beneficial to decrease the vertical tail area and to increase the distance between tether attachment and center of mass.

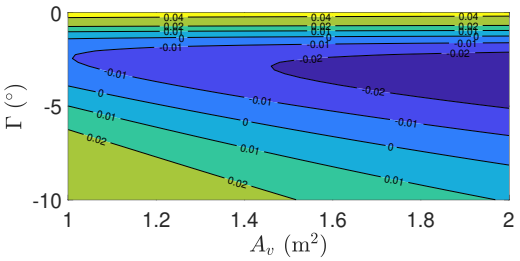

Figure 13. Real part of the pendulum eigenmode at $V_w = 8$ m/s as function of the vertical tail area A_v and the dihedral angle Γ.

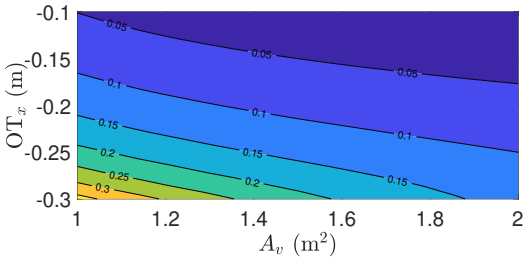

Figure 14. Damping ratio of the phugoid at $V_w = 8$ m/s as function of the vertical tail area A_v and the position of the tether attachment along X_B.

Pendulum and phugoid are both influenced by the sweep angle of the main wing Λ. In Figure 15, eigenvalues are shown as function of this parameter. The pendulum for a sweep smaller than about 3° becomes unstable and splits into two real positive eigenvalues. The phugoid for the same values of sweep moves to the location of the pendulum. This suggests that different eigenmodes can move to the location of the pendulum eigenmode. Therefore, when implementing this problem in an optimization algorithm, care should be given to the tracking and ordering of the eigenvalues: the order of the eigenvalues shall be the same while taking gradients and while performing the optimization steps.

Mass and moments of inertia in a full optimization problem will be linked to the AWES geometry and therefore will be considered as model outputs and not as independent variables. They are here considered as independent variables to study their influence on the eigenmodes. Figure 12 shows that pendulum and phugoid are almost not influenced by the moments of inertia. Moments of inertia will then weakly enter the optimization problem, as they mainly influence eigenmodes which will likely not drive the design.

Among the selected independent variables, OS_z, A_h and AR_h variances almost not influence the eigenvalues and might be fixed in future design and optimization activities. The other independent variables impact the design and therefore should be considered when designing a AWES.

Finally, as Ground-Gen AWESs operate with different tether length during the reel-out phase, eigenvalues should also be studied as function of tether length L_t^0. Figure 16 shows the

dependence of the eigenvalues close to the origin as function of this parameter. The pendulum imaginary part varies according to the approximation given in Eq. (7), while the phugoid gets close the imaginary axis without however largely modifying its damping ratio.

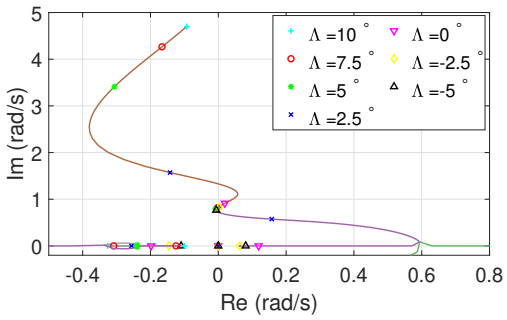

Figure 15. Eigenvalues close to the origin at $V_w = 8$ m/s as function of main wing sweep Λ.

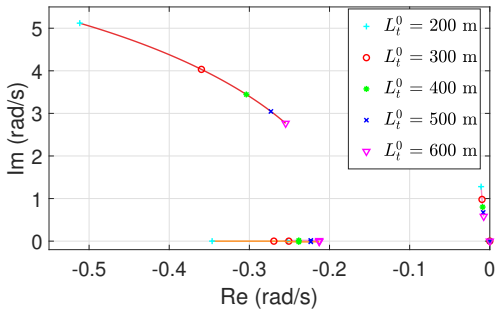

Figure 16. Eigenvalues close to the origin at $V_w = 8$ m/s as function of tether length at rest L_t^0.

5. Conclusions

In this work, the architecture of *T-GliDe* (Tethered Gliding system Design) is introduced with the aid of an example. *T-GliDe* features an optimization module and an uncertainty quantification module. If used together, sensitivity analyses on optimization problems can be performed. If not, an optimal design can be evaluated throughout the optimization module or sensitivity analyses can be performed on a given design throughout the uncertainty quantification module. The optimization problem is built such that an AWES is designed according to market based objective functions, while satisfying constraints related to the flight stability. The modelling approach aims at resolving the flight dynamics without the use of time simulation codes and therefore of active control. Indeed, decoupling the flight dynamics problem from the control problem might allow to identify good designs independently from the use of specific control techniques. To prove this, time simulations of a stable-by-design AWES are currently being performed and will be presented in future works.

An ultra-light aircraft is here used as a Ground-Gen AWES to present trends. A reduced optimization, where only operational design variables are considered, is run to find the optimal working set-points as function of wind speed. The reel-out factor and the pitch angle as function of wind speed are considered as design variables and they are optimized to maximize the capacity factor. Trends of relevant outputs are shown as function of wind speed. In particular, the rigid body eigenvalues are shown and a qualitative description of their trends is given.

The system at $V_w = 8$ m/s is analysed further and a variance based sensitivity analysis is performed to evaluate how the real and imaginary part of the rigid body eigenvalues are influenced by a set of independent variables. Focus is given on the pendulum and phugoid eigenmodes, as they have a small damping ratio. Indeed, in a full optimization these two modes will likely be constrained, driving the aero-structural design. Among the chosen independent variables, a sub-set of variables which bear an impact on the dynamics is identified and they will be considered in future design and optimization activities as design variables.

References

[1] Chris Vermillion, Mitchell Cobb, Lorenzo Fagiano, Rachel Leuthold, Moritz Diehl, Roy S. Smith, Tony A. Wood, Sebastian Rapp, Roland Schmehl, David Olinger, and Michael Demetriou. Electricity in the air:

Insights from two decades of advanced control research and experimental flight testing of airborne wind energy systems. *Annual Reviews in Control*, 52:330–357, 2021.

[2] Filippo Trevisi, Alessandro Croce, and Carlo E. D. Riboldi. Flight Stability of Rigid Wing Airborne Wind Energy Systems. *Energies*, 14(22), 2021.

[3] Florian Bauer, Ralph M. Kennel, Christoph M. Hackl, Filippo Campagnolo, Michael Patt, and Roland Schmehl. Drag power kite with very high lift coefficient. *Renewable Energy*, 118:290–305, 2018.

[4] Filippo Trevisi, Mac Gaunaa, and Michael McWilliam. Configuration optimization and global sensitivity analysis of Ground-Gen and Fly-Gen Airborne Wind Energy Systems. *Renewable Energy*, 178:385–402, 2021.

[5] Urban Fasel, Dominic Keidel, Giulio Molinari, and Paolo Ermanni. Aerostructural optimization of a morphing wing for airborne wind energy applications. *Smart Materials and Structures*, 26:095043, 2017.

[6] Ashwin A. Candade, Maximilian Ranneberg, and Roland Schmehl. Structural analysis and optimization of a tethered swept wing for airborne wind energy generation. *Wind Energy*, 23(4):1006–1025, 2020.

[7] Dylan Eijkelhof. Design and Optimisation Framework of a Multi-MW Airborne Wind Energy Reference System. Master's thesis, Delft University of Technology, Technical University of Denmark, 2019.

[8] fmincon. `https://it.mathworks.com/help/optim/ug/fmincon.html`, 2022 (accessed January 11, 2022).

[9] Jan Roskam. *Airplane Design*. Kansas: The University of Kansas Lawrence, 1985.

[10] Filippo Trevisi, Mac Gaunaa, and Michael McWilliam. Unified engineering models for the performance and cost of Ground-Gen and Fly-Gen crosswind Airborne Wind Energy Systems. *Renewable Energy*, 162:893–907, 2020.

[11] Rolf H. Luchsinger. Pumping Cycle Kite Power. In Uwe Ahrens, Moritz Diehl, and Roland Schmehl, editors, *Airborne Wind Energy. Green Energy and Technology. Springer, Singapore*, pages 47–64. 2013.

[12] Katherine Dykes. Optimization of Wind Farm Design for Objectives Beyond LCOE. *Journal of Physics: Conference Series*, 1618(4):042039, 2020.

[13] Stefano Marelli and Bruno Sudret. UQLAB: a framework for Uncertainty Quantification in MATLAB. *The 2nd International Conference on Vulnerability and Risk Analysis and Management (ICVRAM 2014)*, pages 2554–2563, 2014.

[14] Ilya M. Sobol. Sensitivity analysis for nonlinear mathematical models. *Mathematical Modeling & Computational Experiment*, pages 407–414, 1993.